Tectonophysics, 200 (1991) 79–96
Elsevier Science Publishers B.V., Amsterdam

Experimental deformation of a glassy basalt

Bradley R. Hacker [1] and John M. Christie
Department of Earth and Space Sciences, University of California, Los Angeles, CA 90024-1567, USA

(Received May 4, 1991; revised version accepted June 14, 1991)

ABSTRACT

Hacker, B.R. and Christie, J.M., 1991. Experimental deformation of a glassy basalt. *Tectonophysics*, 200: 79–96.

Deformation experiments were conducted with the intention of identifying how the mechanical behavior and deformation microstructures of a basalt are influenced by the presence of glass that can crystallize to metamorphic minerals or flow. A glassy plagioclase-rich basalt was tested for periods of up to 649 hours at temperatures of 675–875°C, a confining pressure of 1.0 GPa, and strain rates of 10^{-4}–10^{-7} s^{-1}. Over the whole range of experiments, the basalt deformed ductilely in mechanical and textural steady state. At low temperatures (675–775°C), plagioclase crystals deformed by microcracking and twinning, and the glass did not flow into intracrystalline cracks. At higher temperatures (825–875°C), the samples were notably weaker, plagioclase crystals deformed by twinning and dislocation glide, and the glass flowed into cracks. In all samples that were tested for more than 30 hours, neoblasts of dark mica and quartz crystallized at the expense of K-rich glass + enstatite + H_2O. This neomineralization did not affect the strength of the basalt, presumably because it affected only ~ 50 vol.% of each sample. Changes in plagioclase deformation mechanism from twinning and microcracking at fast strain rates to dislocation glide at slow strain rates, may, however, reflect an increase in effective pressure caused by crystallization of the glass.

Introduction

This paper presents mechanical, microstructural, and microchemical data collected during experimental deformation of a glassy basalt that was undergoing metamorphism. The objectives of the study were to (1) determine how the presence of glass affects the mechanical behavior and microstructures of basalt; and (2) identify whether crystallization of the glass affects the mechanical behavior or microstructures. In this paper, "brittle" and "ductile" refer to deformation that is localized or homogeneous, respectively, and "cataclasis" and "crystal plasticity" refer to grain-scale deformation mechanisms involving cracking and sliding of fragments or the movement of dislocations, respectively.

Basaltic rocks vary systematically in their phase proportions and compositions with changes in metamorphic conditions (e.g., pressure and temperature), and consequently, their mechanical behavior and deformation mechanisms should change with conditions of metamorphism. During our experiments, the basalt did partially transform through the reaction K–Al–Si glass + enstatite + $H_2O \rightarrow$ mica + quartz, but for reasons described below, this transformation did not go to completion and some glass remained in all samples. Phase equilibrium experiments suggest that at the conditions of our experiments a basalt might either melt or crystallize minerals from the glass. Tholeiitic basalt melts in the presence of excess water at a temperature of ~ 625°C at a pressure of 1.0 GPa (Stern et al., 1975). All our experiments were conducted at higher temperatures, but were not completed in the presence of excess water because the 0.5 wt.% water we added was probably consumed during metamorphism (see below). However, it is likely that in some of our experiments the glassy basalt was above the

[1] Present address: Department of Geology, Stanford University, Stanford CA 94305-2115, U.S.A.

solidus—and we did find mechanical and microstructural evidence of melting. We also observed crystallization of biotite + quartz in our glassy basalt as might be expected because of the high temperatures (cf. Peterson and Newton, 1990). Peterson and Newton (1990) showed that in a synthetic K_2O–MgO–Al_2O_3–SiO_2–H_2O system, melting of biotite + quartz occurs at 820°C at 1.0 GPa pressure. Thus the biotite + quartz that crystallized in our samples may have melted at temperatures > 800°C.

Although rocks of basaltic composition are common in oceanic crust and lower continental crust, their mechanical properties are poorly understood. Deformation experiments have been conducted on the main constituents of our basalt —plagioclase (Borg and Heard, 1969, 1970; Marshall and MacLaren, 1977a, 1977b; Tullis and Yund, 1977, 1980, 1987; Dell'Angelo et al., 1987; Dell'Angelo and Tullis, 1988) and pyroxene (Avé Lallement, 1978; Kollé and Blacic, 1982, 1983; Kirby and Kronenberg, 1984)—and we compare

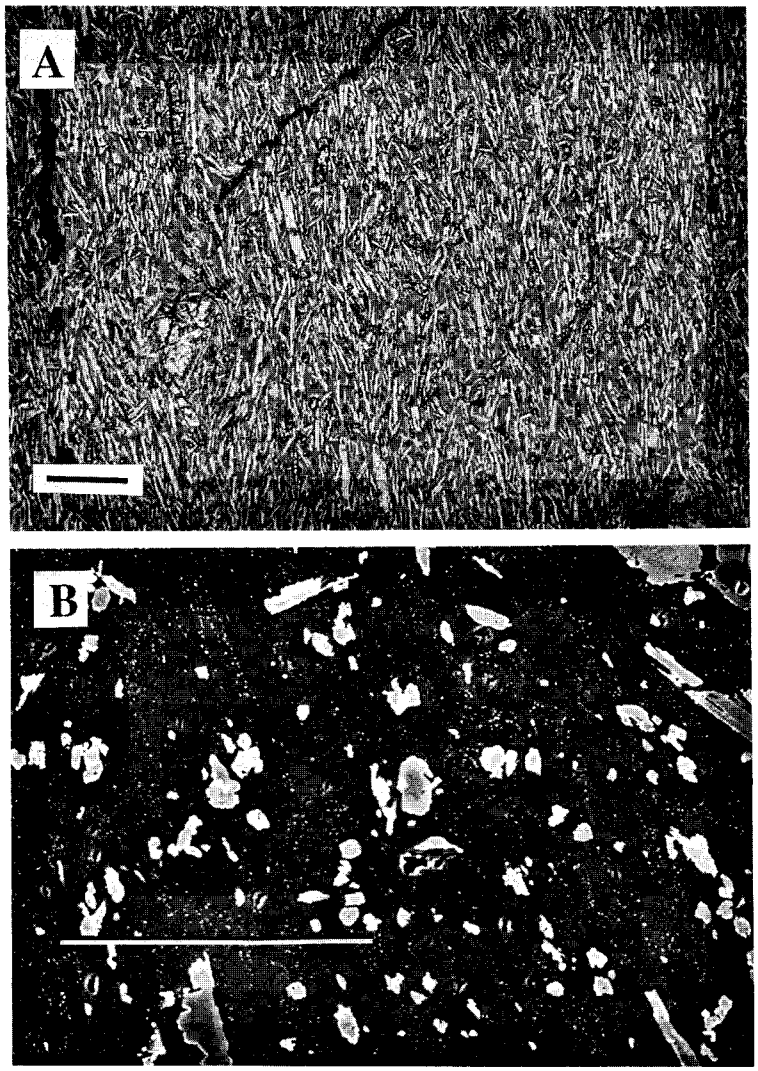

Fig. 1. Starting material; scale bars are 100 μm. (A) Transmitted-light optical photomicrograph. Pale low-relief crystals are plagioclase, high-relief crystals are pyroxene and dark material is glass. (B) Back-scattered electron micrograph. The prominent pale phenocrysts are pyroxene and the dark material is feldspar and glass dotted with tiny bright spinels.

the results of our experiments with these previous studies. Results of experiments on the mechanical behavior and microstructures of holocrystalline pyroxene diabase reported by Kronenberg and Shelton (1980) are also compared with our experiments.

The mechanical and microstructural effects of partial melt have been studied in a variety of rock types (Avé Lallement and Carter, 1970; Van der Molen and Paterson, 1979; Cooper and Kohlstedt, 1984; Dell'Angelo and Tullis, 1988), and our experiments bear comparison with these investigations. Our study is somewhat different than previous studies of partial melting in that the melt in the glassy basalt is already distributed throughout the sample. No time is required for melt to become distributed through the sample—a distribution that may require more than 10 days in samples of non-glassy rock (Dell'Angello and Tullis, 1988).

Experimental procedure

Starting material

The starting material is a two-pyroxene tholeiitic basalt (sample PV-7) from the Panamint Valley of southern California, U.S.A. (Fig. 1; Table 1). It is composed of roughly 8 vol.% phenocrysts (1% olivine, 1% clinopyroxene, 3% orthopyroxene, and 3% plagioclase), and 92% finer grained groundmass. The groundmass contains evenly distributed 60–65% plagioclase, 9% sanidine, 6% orthopyroxene, 6% clinopyroxene, 3% spinel, 1% apatite, and 10–15% glass. The feldspar and pyroxene crystals form a flow foliation.

Olivine phenocrysts are Fo_{88}, subhedral, equant glomerocrysts ≤ 1.5 mm in diameter. Some are rimmed by orthopyroxene. Orthopyroxene phenocrysts are subhedral laths or prisms of enstatite, average 300 μm in length, and contain

TABLE 1

Compositions of phases in the starting material *

	Olivine	Pheno. Opx	G'mass Opx	Pheno. Cpx	G'mass Cpx	Spinel	Pheno. Plag.	G'mass Plag.	Sanidine	Glass
SiO_2	40.44	53.54	56.66	52.09	51.90	0.05	54.96	57.29	63.89	76.5
Al_2O_3	0.05	2.01	0.96	1.94	1.89	10.21	27.36	25.32	18.40	13.0
TiO_2	b.d.	0.36	0.17	0.47	0.83	1.65	0.07	0.10	0.23	1.0
FeO *	11.78	15.01	8.21	5.55	12.33	33.26	0.72	0.73	0.56	1.4
Cr_2O_3	0.05	0.06	0.18	0.42	0.07	39.13	0.06	0.05	b.d.	0.05
MnO	0.26	0.54	0.16	0.18	0.42	0.41	b.d.	b.d.	b.d.	0.05
MgO	47.24	26.01	32.13	16.90	15.29	8.26	b.d.	b.d.	b.d.	0.05
CaO	0.14	2.15	1.42	20.53	16.71	0.06	10.15	8.24	1.12	0.40
Na_2O	b.d.	b.d.	b.d.	0.29	0.35	b.d.	5.45	6.51	4.99	2.4
K_2O	b.d.	b.d.	b.d.	b.d.	0.32	b.d.	0.52	0.70	8.24	5.0
Sum	99.96	99.69	99.89	98.37	100.10	93.03	99.27	98.94	97.45	96.0
Si	1.00	1.94	1.98	1.94	1.96	0.00	2.50	2.61	2.97	
Al	0.00	0.03	0.02	0.03	0.04	0.45	1.47	1.36	1.01	
Ti	b.d.	0.01	0.00	0.01	0.02	0.05	0.00	0.00	0.01	
Fe^{3+}	n.d.	n.d.	n.d.	n.d.	n.d.	0.40	0.03	0.03	0.02	
Cr	0.00	0.00	0.01	0.00	0.00	1.15	0.00	0.00	b.d.	
Fe^{2+}	0.24	0.46	0.24	0.17	0.37	0.63	n.d.	n.d.	n.d.	
Mn	0.01	0.02	0.00	0.01	0.01	0.01	b.d.	b.d.	b.d.	
Mg	1.74	1.41	1.67	0.94	0.86	0.46	b.d.	b.d.	b.d.	
Ca	0.00	0.08	0.05	0.82	0.67	0.00	0.50	0.40	0.06	
Na	b.d.	b.d.	b.d.	0.02	0.03	b.d.	0.48	0.57	0.45	
K	b.d.	b.d.	b.d.	b.d.	0.02	b.d.	0.03	0.04	0.49	

* Pheno. = phenocryst, G'mass = groundmass crystal, Opx = orthopyroxene, Cpx = clinopyroxene, n.d. = not determined, b.d. = below detection. The glass composition was calculated by a method discussed in the text.

rare chromite crystals. Zoning of the orthopyroxene crystals is common and consists of one to three normally zoned overgrowths (with decreasing Mg from core to rim). For example, in one crystal the composition varies smoothly from En_{77} to En_{82} and then changes abruptly back to En_{77}; this cycle is repeated three times. Groundmass orthopyroxene crystals are slightly more calcic enstatite than the orthopyroxene phenocrysts. Clinopyroxene phenocrysts are subhedral augite laths that average 100 μm in length. Groundmass clinopyroxenes are augite to sub-calcic augite. The groundmass pyroxenes are 10–30 μm in length. The spinel grains comprise both chromite and magnetite, are ~ 0.25 μm in diameter, and are spatially associated with ~ 0.1 μm apatite crystals.

Plagioclase phenocrysts are subhedral to euhedral andesine laths as long as 1.0 mm, averaging 400 μm in length. The groundmass plagioclase is also andesine, and occurs as subhedral laths, 50–75 μm in size. None of the plagioclase crystals possesses optically visible undulatory extinction, and transmission electron microscopy (TEM) reveals common growth twins spaced ~ 0.15 μm apart, and a density of free dislocations less than 10^6 cm^{-2}. The plagioclase has $C\bar{1}$ symmetry and contains sub-microscopic (~ 10 Å) phase modulation (e-type superstructure) that is common in intermediate plagioclases (Nissen, 1974). Sanidine occurs as subhedral laths 5–10 μm long. None of the sanidine crystals has optically visible undulatory extinction or twins.

Glass analyses require special interpretation because the glass pools are smaller than the minimum excitation volume during electron-probe microanalysis (~ 2 μm), and adjacent crystals contribute to the analyses. By plotting analyzed glass compositions versus total oxide concentration, and assuming that the analyses with the totals nearest 100 wt.% are most contaminated by adjacent feldspar crystals, one can estimate the true glass composition (Table 1). An alternative method, plotting analyzed glass compositions relative to feldspar compositions, yields similar results. The starting material contains no hydrous phases other than glass, and it does not contain quartz.

Experimental apparatus

The experiments were conducted in a piston-cylinder, solid-pressure-medium rock-deformation apparatus of the type designed by Griggs and coworkers (Griggs, 1967; Blacic, 1971). Each experiment was taken to the desired pressure and temperature along a path such that the specific volume of free H_2O remained less than one, and was then left undisturbed for ~ 12 hours before the deformation experiment began.

The samples were right circular cylinders, 6.25 mm in diameter and 12.7 mm in length. This sample size yielded approximately 100 groundmass grain diameters across the sample diameter. The sample was placed inside a 0.125 mm-thick cylindrical silver jacket surrounded by a confining medium of talc (fig. 6 of Hacker and Christie, 1990). The 0.5 wt.% water added was pipetted onto the top of the sample after the sample had been inserted into the silver jacket. During pressurization, the jacket was compressed against the two ceramic end-pieces, mechanically sealing the water in the jacket. The effectiveness of this seal is not quantitatively known, but, quartzose rocks tested in identical assemblies at similar conditions in our laboratory are damp at the end of experiments, indicating that some water remains in contact with the sample during the experiments. The loss of water through the jacket is impeded by dehydration of talc in the surrounding pressure medium. The basalt samples were not damp at the end of the experiments, but they did show obvious textural changes indicating elevated water activity (principally mica growth).

The temperature was provided by resistive heating of a stepped cylindrical graphite furnace surrounding the sample and confining medium, and was measured by two $Pt/Pt_{90}Rh_{10}$ thermocouples. Temperature control was better than ± 3°C precision for most experiments. Temperatures were not corrected for pressure or differential stress effects on the thermocouple e.m.f., which should result in an uncertainty of ± 4–6°C for temperatures of 675–875°C at a confining pressure of 1.0 GPa (Getting and Kennedy, 1970; Mao and Bell, 1971). The experiments were

quenched rapidly: an experiment at 900°C cooled to 400°C in 10 s and 225°C in 20 s. The thermal profiles in the assemblies used in this study should be similar to those presented by Koch et al. (1989). The temperatures reported here are for the center of the sample; thermocouple temperatures are ~25°C lower. The confining pressure measured was not corrected for friction within the assembly or strength of the confining medium.

The output from the displacement transducers, force gauge, pressure gauge, and one thermocouple, was monitored by a Molytek datalogger/recorder. The datalogger/recorder printed all information on a strip chart, and transmitted it serially to a Macintosh microcomputer. The computer (1) received and deciphered the serial transmissions from the datalogger/recorder; (2) stored the transmitted data magnetically on disk; and (3) immediately calculated and displayed real-time stress–strain curves, allowing continuous evaluation of experiments in progress. After the completion of experiments, the data on disk were reanalyzed to allow more precise calculations. Strain and strain rates were calculated from the displacements measured by two displacement transducers, correcting for apparatus distortion and changes in sample diameter during deformation. Uncertainty introduced in the strain measurement by the apparatus-distortion calibration and nonlinearity of the displacement transducers is estimated to be less than 0.5%. The differential stress was calculated as the difference between the axial stress and the confining pressure, and corrected for apparatus distortion and changes in sample diameter during deformation. The samples showed minimal barreling, and the uncertainties in the calculated strains and stresses are estimated to be ~10%.

Analytical methods

After each experiment terminated, the sample jacket was carefully removed, incrementally, with a lathe. Chemical treatment to remove the jacket or confining medium was specifically avoided to prevent contamination of the sample. The sample was then impregnated with resin and sawed in half. One doubly polished 30-μm section of every sample was made for examination by optical microscopy, back-scattered electron microscopy (BSEM), and electron-probe microanalysis. Additional doubly polished < 30 μm sections of selected samples were made and thin foils prepared for examination by TEM.

Textural observations and chemical analyses of the phases were all made with a four-spectrometer Cameca Camebax electron-probe microanalyser and a single set of well-characterized natural and synthetic mineral standards. Spot selection and textural analysis were performed in the back-scattered electron mode to ensure that only single phases were analyzed, and to facilitate the identification of compositional zoning. The electron beam diameter was 2 μm, at 15 kV and 10 nA. Count times for each analysis were 20 s for peak intensities and 10 s for background intensities. Detection limits at these conditions are a function of phase composition, but for this study, conservative limits for crystalline phases are approximately 0.02 wt.% for SiO_2, Al_2O_3, TiO_2, Cr_2O_3, and MnO, 0.03 wt.% for FeO*, MgO, and CaO, 0.04 wt.% for K_2O, ad 0.05 wt.% for Na_2O. Analyses of inhomogeneous grains were not averaged, and are presented individually. The apparent volatile contents of the glasses (~5 wt.%) may be a result of using mineral standards, or it could be that the quenched melts actually contain ~5 wt.% volatiles; the solubility of H_2O-rich fluid in tholeiitic glass quenched from pressures of ~1.0 GPa is ~10 wt.% (Merzbacher and Eggler, 1984). It was not possible to use broad-beam techniques to measure glass compositions because the glass regions were all smaller than the diameter of the electron probe.

A JEOL JEM 100-CX TEMSCAN scanning/transmission electron microscope, equipped with a beryllium double-tilt goniometer stage was used for phase identification and to characterize microstructures.

Results

Experiments were conducted for periods of up to 649 hours at temperatures of 675–900°C, a confining pressure of 1.0 GPa, and strain rates of 10^{-4}–10^{-7} s^{-1} (Table 2). The slowest and hottest

experiment with a flow stress measurable in the apparatus was conducted at 900°C and 10^{-6} s^{-1}. The fastest and coolest experiment with a flow stress less than the strength of the pistons was conducted at 675°C and 10^{-5} s^{-1}. All experiments were conducted with 0.5 wt.% water added to promote metamorphic reactions.

Metamorphism

No compositional or mineralogical changes were recognized in samples deformed for less than 30 hours (10^{-4} and 10^{-5} s^{-1} strain rates), although any change that might have occurred would be difficult to recognize because of the

TABLE 2

Experimental conditions and results *

T (°C)	Strain rate (s^{-1})	P_c (GPa)	P (GPa)	Stress (MPa)	Strain (%)	Time (hour)	Contains Qtz + mica	Experiment No.
675		1.00	1.33	high friction	26	50	yes	1249
675	2.1×10^{-4}	0.99	1.17	1440	40	52	yes	1265 [1]
675	1.8×10^{-5}	0.98	1.69	2120	30	32	no	1241
675	1.8×10^{-5}	1.00	1.64	1915	46	31	yes	1250
675	1.9×10^{-5}	0.99	1.17	1030	40	52	yes	1265 [1]
675	1.9×10^{-6}	0.99	1.30	908	29	62	yes	1232
675	1.7×10^{-6}	0.99	1.17	515	40	52	yes	1265 [1]
675	1.6×10^{-6}	0.99	1.49	1500	26	71	yes	1270
675	1.3×10^{-6}	1.01	1.46	1360	10	76	yes	1276
675	1.6×10^{-7}	1.00	1.33	990	24	649	yes	1245
725	1.7×10^{-4}	0.99	1.32	2200	60	62	yes	1268 [2]
725	1.4×10^{-4}	1.02	1.54	2480	16	22	no	1274 [3]
725	1.6×10^{-5}	0.99	1.32	1600	60	62	yes	1268 [2]
725	1.9×10^{-5}	1.02	1.54	1580	16	22	no	1274 [3]
725	1.5×10^{-6}	0.99	1.32	980	60	62	yes	1268 [2]
775	1.7×10^{-4}	1.03	1.44	1246	28	17	no	1243
775	1.7×10^{-4}	0.98	1.40	1850	32	27	no	1248 [4]
775	1.7×10^{-4}	1.00	1.25	1700	45	73	yes	1266 [5]
775	1.7×10^{-5}	0.99	1.46	1390	28	26	no	1240
775	1.7×10^{-5}	0.98	1.40	1230	32	27	no	1248 [4]
775	1.7×10^{-5}	1.00	1.25	1230	45	73	yes	1266 [5]
775	1.8×10^{-6}	1.05	1.26	690	25	59	yes	1231
775	1.7×10^{-6}	1.00	1.25	755	45	73	yes	1266 [5]
775	1.9×10^{-7}	1.00	1.18	525	13	520	yes	1271
825	1.5×10^{-6}	1.00	1.12	360	63	74	yes	1269
825	1.5×10^{-4}	0.99	1.26	790	34	24	no	1273 [6]
825	1.7×10^{-4}	0.99	1.06	815	30	74	yes	1275 [7]
825	1.6×10^{-5}	0.99	1.26	380	34	24	no	1273 [6]
825	1.5×10^{-5}	0.99	1.06	390	30	74	yes	1275 [7]
825	1.6×10^{-6}	0.99	1.26	170	34	24	no	1273 [6]
825	1.7×10^{-6}	0.99	1.06	190	30	74	yes	1275 [7]
875	1.7×10^{-4}	1.04	1.20	530	28	11	no	1230
875	1.4×10^{-4}	1.00	1.22	670	35	15	no	1242
875	1.6×10^{-4}	1.00	1.09	635	16	20	no	1267 [8]
875	2.2×10^{-5}	1.00	1.11	340	18	20	no	1247 [9]
875	1.9×10^{-5}	1.00	1.11	326	18	20	no	1247 [9]
875	1.6×10^{-5}	1.00	1.09	260	16	20	no	1267 [8]
875	1.9×10^{-6}	1.00	1.06	170	26	63	yes	1246
875	1.7×10^{-6}	1.00	1.06	180	34	53	yes	1252

* P_c = confining pressure, P = mean normal stress, Time = duration of experiment, "Contains Qtz + Mica" = sample contains or does not contain neoblasts of quartz and mica. Superscripts to experiment numbers indicate strain-rate-stepping experiments.

wide compositional variation of zoned pyroxene and feldspar crystals in the starting material. Moreover, no overgrowths on crystals originally present in the rock were seen.

In all samples that were tested for more than 30 hours (10^{-6} and 10^{-7} s^{-1} strain rates), the glass near the sample edges and along faults crystallized to dark mica and quartz (Fig. 2). The alteration occurred in up to ~ 50 vol.% of each sample. The amount of alteration was not related to the duration of the experiments, suggesting that the reaction was limited by the amount of added water. The amount of water was insufficient to permit the reaction of all glass to quartz + mica even during the longest experiments.

The dark mica occurs as subhedral lath-shaped overgrowths on enstatite, and has approximate composition $K_{0.9}Mg_{1.3}Fe_{1.4}Ti_{0.2}Al_{0.1}(Al_{0.9}Si_{3.1})O_{10}(OH)_2$. Mica analyses judged to be relatively uncontaminated by adjacent phases are listed in Table 3. The compositions are more siliceous than natural biotites and more ferromagnesian

Fig. 2. Quartz (q) and mica (m) growing at the expense of pyroxene (x), plagioclase (p) and glass (L) in a fault zone in sample GB-1231, strained 25% at 775°C, 1.8×10^{-6} s^{-1} strain rate at 1.05 GPa confining pressure and 690 MPa flow stress over a 59-hour period. (A) Back-scattered electron micrograph, scale 10 μm. (B) Transmission-electron micrograph showing the mica (arrows) and quartz (q) crystals that are the reaction products of pyroxene and glass (not shown). p is plagioclase and the scale is 1 μm.

TABLE 3

Mica compositions *

Run No.:	1250	1245	1245	1270
SiO_2	45.48	38.84	39.74	39.90
Al_2O_3	10.37	11.98	10.83	12.99
TiO_2	1.19	3.97	2.38	3.09
FeO *	9.47	21.96	19.25	17.30
Cr_2O_3	b.d	0.04	0.06	b.d
MnO	0.13	0.18	0.27	0.24
MgO	19.54	9.55	11.62	11.21
CaO	0.37	0.75	0.75	0.59
Na_2O	0.29	0.21	0.21	0.48
K_2O	8.06	8.79	8.86	7.29
Sum	94.90	96.27	93.96	93.11
	Cations per 11 oxygens			
Si	3.32	3.06	3.07	3.04
Al^{IV}	0.68	0.94	0.93	0.96
Al^{VI}	0.22	0.18	0.05	0.20
Ti	0.07	0.24	0.14	0.18
Fe	0.57	1.45	1.28	1.14
Mn	0.01	0.01	0.02	0.02
Mg	2.13	1.12	1.34	1.27
Ca	0.03	0.06	0.06	0.05
Na	0.04	0.03	0.03	0.07
K	0.75	0.89	0.87	0.71

* Fe cations calculated as Fe^{2+}. b.d. = below detection.

than natural muscovites. However, the micas are difficult to analyze by electron probe because they do not polish well and are no larger than a few micrometers across. The quartz crystals are anhedral, ~ 0.2–1.0 μm in diameter, and grew between plagioclase laths in areas formerly occupied by glass. Textural relationships suggest that the reaction was:

K–Al–Si glass + enstatite + H_2O

→ mica + quartz

With the exception of H_2O, which is impossible to measure directly by electron microprobe, the reaction can be balanced roughly (in terms of wt.%) as:

8 glass + 3 enstatite → 4 mica + 6 quartz

The starting material contains glass, and glass is also present in all the deformed samples. Most glass regions were less than 2 μm across, i.e. smaller than the activation area of the electron probe. Because of this it was impossible to conclude whether the glass observed in a deformed sample was quenched melt produced during the experiment or glass originally present in the starting material. It was also not possible to determine by compositional criteria whether the glass attained low enough viscosity to flow during an experiment. However, TEM examination shows that microcracks produced by deformation in experiments at temperatures ≥ 825°C contain glass, whereas cracks produced at lower temperatures are not filled with glass. This suggests that in the higher temperature experiments the glass had low enough viscosity to flow into cracks on the time scale of the experiments. As described below, the basalt samples were also markedly weaker at temperatures ≥ 825°C.

Deformation

Mechanical data

Most of the basalt samples shortened ductilely. The stress supported by each sample reached a relatively constant value at imposed constant strain rate and temperature (Fig. 3), and different samples tested under identical conditions supported similar stresses. Nearly all the stress/strain curves are characterized by an initial "elastic" region of constant slope followed by yielding and a smooth transition to a "steady state" flow stress. This is typical of other unmelted and partially melted feldspathic rocks (e.g., Van der Molen and Paterson, 1979; Tullis and Yund, 1980; Dell'Angelo and Tullis, 1988). There is no weakening or strengthening observed, even in samples strained 60%, compatible with the observation below that the rock texture did not change noticeably with increasing strain.

There are no differences in the morphologies of stress/strain curves obtained at high temperatures (≥ 825°C) compared with low temperature ≤ 775°C) conditions. As stated previously, TEM observations suggest that the glass in the starting material became fluid enough to flow into cracks during experiments at temperatures ≥ 825°C, whereas glass was not noted in cracks at lower temperatures. The measured flow stresses indicate a marked reduction in strength at temperatures ≥ 825°C as well. It is not likely that the strength reductions were caused by dehydration

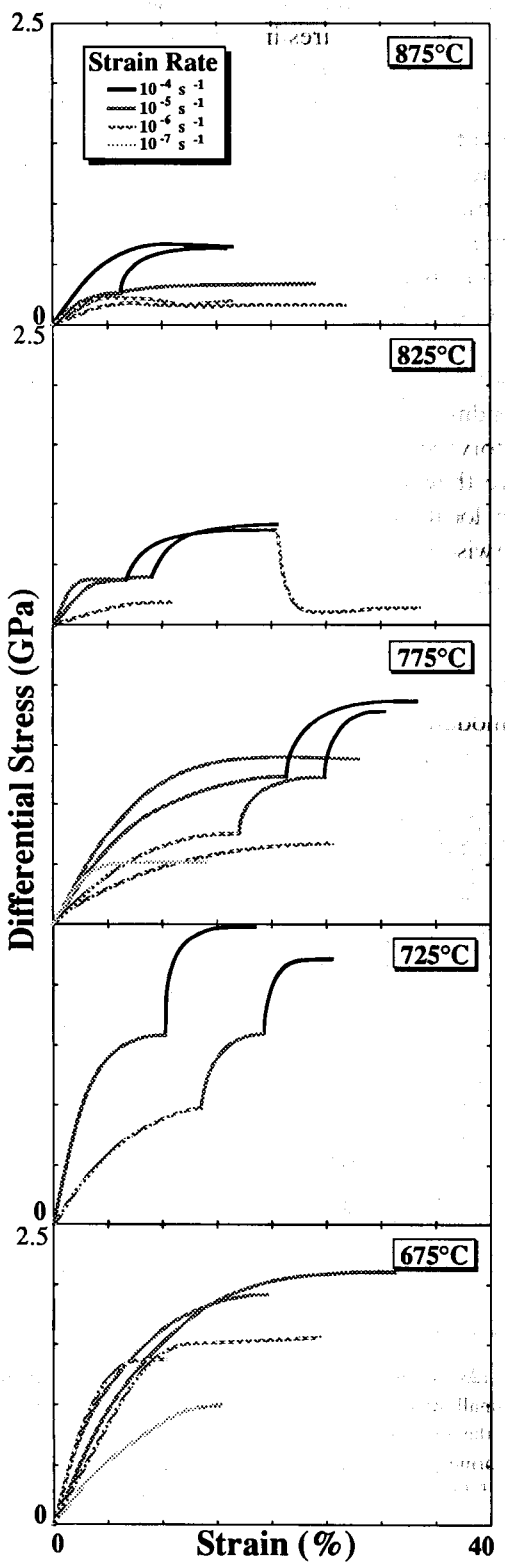

Fig. 3. Axial differential stress vs. axial strain.

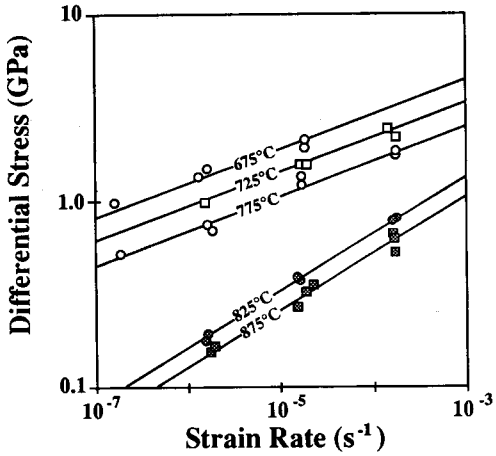

Fig. 4. Power law fit of the mechanical data.

of the talc confining medium at these temperatures, because (1) mica growth occurred in samples heated for 30 hours or more, regardless of temperature; and (2) the higher temperature samples do not contain more mica than the lower temperature samples. Both observations indicate that water produced by talc dehydration outside the sample jacket was not available for mica growth within.

Constitutive relationships

A power-law fit of the relationship between steady state stress (MPa), strain rate (s^{-1}), and temperature (K) for the glassy basalt samples deformed at temperatures of 675–775°C is $\dot{e} = 5.3 \pm 1.0 \times 10^{-9}\ \sigma^{5.4 \pm 0.2}$ exp. $-263 \pm 20/RT$, where the activation enthalpy is in kJ mole^{-1} (Fig. 4). The glass in these samples remained viscous enough not to flow into open cracks in plagioclase crystals. A similar power-law fit for the samples deformed at temperatures of 825–875°C is $\dot{e} = 1.1 \pm 0.1 \times 10^{-5}\ \sigma^{3.3 \pm 0.1}$ exp. $-175 \pm 30/RT$ (Fig. 4). The glass in these higher temperature samples attained low enough viscosity that it was able to flow into cracks. The quoted uncertainties indicate only the ability of the power-law equation to fit the data, and do not incorporate uncertainties in the measured stresses, strain rates, and temperatures. The values of steady state stress used in the regression fitting were taken from at least one single-strain-rate, single-temperature test for each tempera-

ture/strain-rate point. A second value for each strain rate of 10^{-4} to 10^{-6} s^{-1} was taken from a strain-rate stepping test. An experiment was excluded from regression fitting if high piston friction prevented identifying when the piston contacted the sample.

Microstructures

Deformation of the basalt occurred by a combination of cracking and dislocation glide within crystals, slip along grain-scale faults, and flow within the glass. Over the whole range of experiments the basalt was ductile (i.e., the samples shortened homogeneously). Each sample contains a network of ~10–100 interpenetrating microfaults 1–20 μm wide, typically inclined at 40–50° from the compression axis. The faults are difficult to observe optically, but an exceptionally well-developed example is illustrated in Fig. 5. Fault zones imaged in TEM contain angular fragments that range from $\leq$ 10 nm to 1 μm in diameter (Fig. 5). Between subparallel fault strands, subequant pyroxene crystals appear to have rotated and developed tails composed of comminuted fragments. Feldspar crystals either rotated and slipped along fractures in a sense opposite to that of the bounding fault strands, or bent at their ends by microcracking or dislocation glide in the direction of fault movement; bending is more prevalent than grain-scale cracking. Thus the deformation, though ductile on the scale of the samples, is cataclastic within the fault zones.

Little of the sample deformation was accommodated by the phenocrysts, which make up only ~8% of the rock volume. The phenocrysts behaved as relatively rigid objects in a softer groundmass. In general, phenocrysts possess undulatory extinction and/or grain-scale cracks only where they are in contact with other phenocrysts or in local displacement gradients near pistons; otherwise they appear undeformed optically.

Virtually all the deformation of the samples was accommodated by the fine-grained material in the groundmass. One might expect that much of the deformation of the groundmass was accommodated by the glass, because the glass is

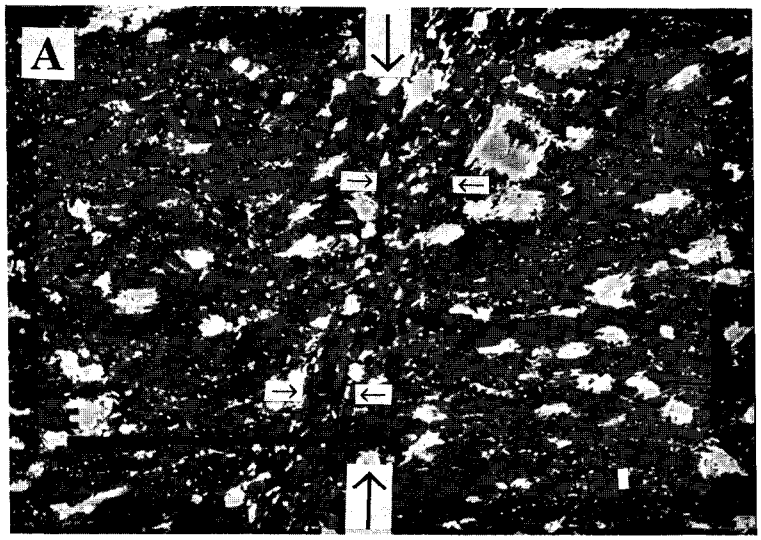

Fig. 5. Fault zones. (A) Back-scattered electron micrograph of sample GB-1231 strained 25% at 775°C, 10^{-6} s^{-1} strain rate and 690 MPa flow stress over a 59-hour period. The fault zone is indicated by small arrows and the compression direction was parallel to the large arrows; scale is 100 μm. Quartz is more abundant along the fault zone, suggesting that the quartz-producing metamorphic reaction (by crystallization of glass) was enhanced in the deformed region (cf. Fig. 2). Note that although the fault zone is oriented ~20° to the compression axis, the cracks within individual feldspar crystals are perpendicular to the compression axis. (B) Transmission-electron micrograph of sample GB-1241 strained 35% at 675°C, 10^{-4} s^{-1} strain rate and 670 MPa flow stress over a 15-hour period; scale is 1 μm. Plagioclase at top of photo is cracked and at the bottom of the photo is finely comminuted.

probably the weakest phase in the rock (Hacker et al., 1987), and even those areas of glass that crystallized to mica + quartz are expected to be weaker than all the other crystalline phases (e.g., Dell'Angelo and Tullis, 1989; Shea and Kronenberg, 1989). It was, however, impossible to quantify the deformation of the groundmass glass, because the glass does not contain indicators of deformation such as flow banding. We evaluated whether melt redistribution occurred during our experiments by measuring (by the method of linear intercepts) the spacing between plagioclase microlites at the top, bottom, sides, and center of each specimen. Within uncertainty, the crystal spacing is identical at different places within individual samples, and among different samples deformed at different temperatures and strain rates. Moreover, the glass does not form elongate pools parallel to the compression axis or pools adjacent to the sample jacket. This suggests that the melt was not very mobile during the experiments and a steady-state texture was maintained.

A transition in microstructures of groundmass plagioclase crystals occurs with decreasing strain rate and, to a lesser extent, with increasing temperature. Groundmass plagioclase crystals in samples deformed at fast strain rates contain microcracks and twins (Fig. 6). At the lowest temperature (675°C) and fastest strain rate (10^{-5} s^{-1}), dislocations are uncommon. Dislocations are present at higher temperatures and fast strain rates, but they are not predominant. Twinning and microcracking are inferred to have occurred concurrently, because some twins appear to have nucleated along cracks while others are offset along cracks. Both albite and pericline mechanical twins are present. Cracked grains often contain two sets of microcracks inclined ~45° to the compression axis—the same geometry of grain-scale faults observed with optical microscopy (Fig. 6). These microcracks are ~2–8 μm wide and spaced ~0.3–1.0 μm apart. Most of the fractures observed optically within plagioclase crystals are oriented parallel to the compression axis,

Fig. 5 (continued).

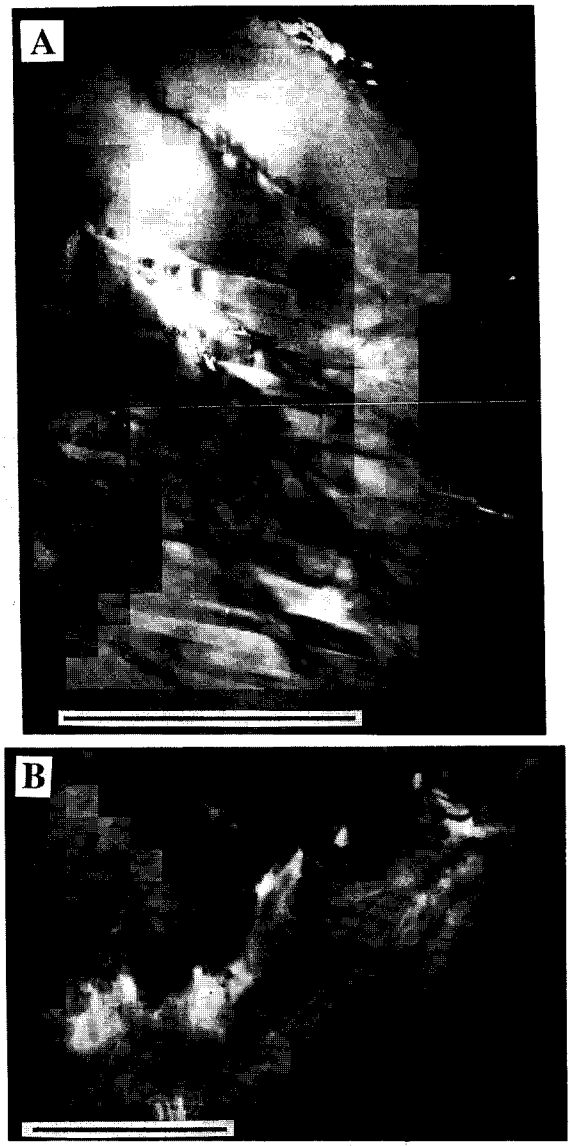

Fig. 6. Transmission-electron micrographs of plagioclase crystals in sample GB-1252 strained 34% at 875°C, 1.7×10^{-6} s^{-1} strain rate, 1.00 GPa confining pressure and 180 MPa flow stress over a 53-hour period; scale bars 1 μm. (A) Mechanical twins and en-echelon microcrack array. (B) Dislocation loops, curved dislocations and straight dislocations parallel to the trace of the (010) plane.

that is, they are extension fractures. At slow strain rates, cracking is less common, and groundmass plagioclase crystals contain predominantly dislocations. The dislocation density varies from $\leq 10^{10}$ cm^{-2} at 675°C to $\leq 10^{9}$ cm^{-2} at 875°C. Some strongly curved dislocations indicate that climb may have occurred (Fig. 6), but some cracking occurred even at the highest temperature. The neomineralized quartz and mica in the groundmass invariably lack dislocations.

Discussion

Effect of metamorphism

One objective of this study was to identify whether metamorphic changes during the duration of a laboratory experiment could affect the mechanical behavior or microstructures of glassy basalt. Growth of dark mica and quartz replacing glass was visible in all samples that were tested more than 30 hours. No mechanical changes appear to be associated with this transformation, but the change in plagioclase microstructures from dominantly cracking and twinning to dominantly dislocation glide may be a result of this transformation. The lack of a mechanical effect may be because the neomineralization affected only ~ 50 vol.% of each sample; had 100 vol.% of the sample glass transformed to mica and quartz, mechanical changes might have been observed. The presence of glass may have reduced the effective pressure and caused microcracking of plagioclase, whereas the crystallization of quartz and mica probably suppressed the pressure reduction caused by the glass and reduced plagioclase microcracking.

Effect of partial melting

The deformation mechanisms operative in a partially melted rock can be complex. The constituent grains can slide past one another or deform by fracture, dislocation glide or diffusion. The melt can be a passive medium through which the grains slide, it can transport diffusing species, and it can promote cracking by reducing effective pressure. Various combinations of these deformation mechanisms have been noted in partially melted rocks tested in the laboratory. Dell'Angelo and Tullis (1988) studied the effects of partial melt on the deformation of sintered and natural aplite that deformed by dislocation creep in the absence of melt. They found that the deformation mechanisms depended on the grain size, strain rate, and the proportion of melt. For example, in

an aplite with 10 vol.% melt shortened at 10^{-6} s^{-1} strain rate, the melt was squeezed to the edges of the sample and deformation occurred by dislocation creep. At 15 vol.% melt or 10^{-5} s^{-1} strain rate, cataclasis occurred. They suggested that the melt could not flow rapidly enough at the faster strain rates and consequently high fluid pressures develops Cooper and Kohlstedt (1984) made a similar interpretation of the effect of basaltic melt on dunite.

In the glassy basalt of this study, deformation occurred by movement of melt (indicated by glass-filled cracks in feldspar crystals), cracking of grains, dislocation glide in grains, and sliding of grains past one another. The relative importance of these mechanisms depended on strain rate and temperature. The high strain-rate sensitivity of the flow stress ($n = 3.3$) suggests that dislocation glide or deformation of thin melt films (and not cracking) controlled the rate of deformation. Apparently, the melt volume was small enough that the stresses were transmitted through the framework grains, and the rheology of the samples was dominated by the framework grains. Melt-assisted diffusion creep appears not to have been important, except perhaps in the neomineralized quartz and mica grains, which lack dislocations and cracks and are very fine grained.

Previous partial melting studies on lherzolite (Avé Lallement and Carter, 1970), granite (Van der Molen and Paterson, 1979), and aplite (Dell'Angelo and Tullis, 1988) noted that grain-boundary melt films may be thickest parallel to the compression direction, and thinnest in orthogonal orientations. Although the glassy basalt samples were deformed to similar strains in this study, no similar anisotropic melt distribution was observed, suggesting that textural steady state was achieved. Cooper and Kohlstedt (1984) performed experiments on olivine aggregates that they inferred were able to remain texturally equilibrated with basaltic melt, but their samples deformed by diffusional creep.

Comparison with unmelted feldspathic rocks

The only other extensive study of ductility in plagioclase–pyroxene rock is Kronenberg and Shelton's (1980) investigation of Maryland diabase. The mechanical and microstructural characteristics of the glassy basalt can be compared with those of the non-glassy Maryland diabase, to yield further insight into the effect of the presence of glass. Maryland diabase contains pyroxene and plagioclase in a roughly 2:1 ratio, whereas our glassy basalt contains pyroxene and plagioclase in a ratio of $\sim 1:4$. The average grain size in both rocks is similar at ~ 75 μm. At 1.0 GPa confining pressure and a strain rate of 10^{-6} s^{-1}, Kronenberg and Shelton (1980) found faulting at 600°C and ductility at 800°C. The present study extends the domain of ductility at laboratory strain rates down to 675°C; in this sense there is no difference in the behavior of the two rock types. The cause of the ductility is, however, different. Ductility was achieved in the diabase by dislocation glide and twinning at temperatures of 600–900°C at 1.0 GPa confining pressure, whereas in the glassy basalt much of the deformation appears to have been accommodated by flow within the glass or the mica + quartz that crystallized from the glass. Microcracking occurred to higher temperatures in the glassy basalt (875°C) than in the diabase (800°C), presumably because of the presence of melt.

The glassy basalt shares certain microstructural characteristics with dried polycrystalline albite (Tullis and Yund, 1980). At a temperature of 700°C, a pressure of 1.5 GPa, and 10^{-6} s^{-1} strain rate, dry Hale albite shows extensive grain-scale faulting; this also occurs in our samples at 1.0 GPa, and presumably was enhanced by the presence of melt. Both dry Hale albite and glassy basalt have low dislocation densities at these conditions. Wet Hale albite deformed at 700°C contains abundant regions of uniform high dislocation density, not like the glassy basalt. Whereas wet Hale albite tested at 800°C shows abundant recovered and recrystallized zones, the glassy basalt is like dry Hale albite, which shows a range of moderate, inhomogeneous dislocation densities and no recrystallization (Tullis and Yund, 1980).

Compared to unmelted plagioclase-rich rocks such as granite and diabase (Tullis and Yund, 1977; Kronenberg and Shelton, 1980), the mi-

crostructural transition in groundmass plagioclase in the glassy basalt from cracking at low strain rates to dislocation glide at higher strain rates is a stronger function of strain rate and a weaker function of temperature. Dell'Angelo and Tullis (1988) noted for partially melted aplite a similar marked strain-rate dependent change from dislocation creep to cataclasis. In both cases, the plagioclase microstructures probably reflect changes in the relative strengths of plagioclase and melt, which change more rapidly as a function of strain rate than temperature.

The activation enthalpy determined for creep of the glassy basalt at temperatures of 675–775°C (263 ± 20 kJ mole^{-1}) is identical to the activation enthalpies reported for creep of anorthosite (234–238 kJ mole^{-1}; Shelton and Tullis, 1981) and diabase (259 kJ mole^{-1}; Shelton and Tullis, 1981), and significantly less than the activation enthalpy reported for creep of clinopyroxenite (335–380 kJ mole^{-1}; Shelton and Tullis, 1981; Kirby ad Kronenberg, 1984). This suggests that the volumetrically minor pyroxene and glass play less important roles than the more abundant plagioclase in determining the rheology of the glassy basalt at lower experimental temperatures. Moreover, the rate-limiting step may be the same for unmelted plagioclase-rich rocks and partially melted basalt. Cooper and Kohlstedt (1984) found that the presence of 5–15 vol.% basaltic melt increased the diffusion creep rate of dunite by a factor of 2–5, while the stress exponent and activation enthalpy remained unchanged.

The strength of the glassy basalt can be compared to the strengths of other experimentally deformed rocks. A convenient way to illustrate this is to compare the flow stresses for a single temperature. Figure 7 shows the flow stresses for strain rates in the experimental range at 800°C. Note that this temperature is chosen for comparative purposes only, and is outside the range of some experiments on which these extrapolations are based, and outside the thermal stability of some of the rocks. The strength of the glassy basalt extrapolated from experiments at temperatures ≤ 775°C is roughly comparable to the strengths of diabase, anorthosite, albite rock (Shelton and Tullis, 1981), synthetic amphibolite (Hacker and Christie, 1990) and Koch et al.'s (1989) "dry" quartzite.

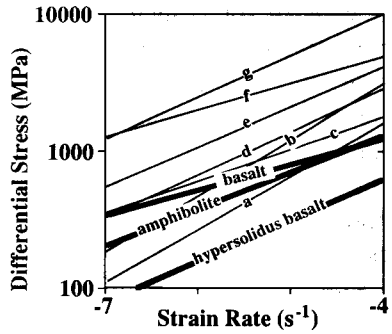

Fig. 7. Flow stresses for various rocks at laboratory strain rates and a temperature of 800°C. 800°C is outside the temperature range of the original experiments for some of these rock types and some of the calculated stresses are unreasonably high. *a* = "wet" quartzite (Koch et al., 1989); *b* = "dry" quartzite (Koch et al., 1989); *c* = albite rock (Shelton and Tullis, 1981); *d* = anorthite rock (Shelton and Tullis, 1981); *e* = diabase (Shelton and Tullis, 1981); *f* = diopside rock (Kirby and Kronenberg, 1984); *g* = harzburgite (Borch and Green, 1989). "Amphibolite" refers to the synthetic amphibolite of Hacker and Christie (1990) and "basalt" is extrapolated from experiments in the present study conducted at temperatures ≤ 775°C.

Orientation of faults

The faults in our samples are oriented $\sim 45°$ to the compression axis, whereas faults in experimental samples are typically inclined $\sim 30°$. Shelton et al. (1981) also noted 45° faults in vacuum-dried albite deformed at 900–1125°C, and suggested that the faults developed as cracks propagating in high resolved shear stress orientations. They noted that high confining pressure should favor the propagation of shear cracks over tensile cracks, which involve a volume increase. Although our experiments were at high confining pressure, which should favor the propagation of shear cracks, the pressure should have been reduced by the presence of the melt. Cracks formed under high fluid pressure will have an extensional orientation. Shelton et al. (1981) also suggested that dislocations may contribute to reductions of tensile stress concentrations at the crack tips, tending to favor shear cracks. They proposed that the high temperatures of their experiments per-

mitted dislocations to glide through asperities and reduce friction along the shear cracks, which nucleated along flaws such as grain boundaries and cleavage planes. This explanation cannot apply to our experiments where the fractures formed parallel to the compression axis because of low melt-induced effective pressure and then coalesced to form 45° faults.

Van der Molen and Paterson (1979) also observed in partially melted granite that trans-granular fractures formed parallel to the compression direction. Moreover, in their samples with > 15 vol.% melt, ill-defined 2–4 mm wide shear zones with cataclastically reduced grain size developed. The shear zones in their specimens that failed at high stresses with < 15 vol.% melt are oriented at high angles (~ 50–$70°$) to the compression axis.

Treatment of the glassy basalt as a two-phase aggregate

It may be possible to treat the mechanical behavior of the glassy basalt as a two-phase aggregate composed of plagioclase and melt, using knowledge of plagioclase and melt rheology (Fig. 8). The viscosity of a rhyolite melt, similar in composition to the melt in the glassy basalt, was measured by Webb and Dingwell (1990). Over a range in strain rates of 10^{-4} to 10^{-7} s^{-1} and temperatures of 650–1000°C, they found that the rhyolite melt was Newtonian, with an activation energy of 444 kJ $mole^{-1}$. At faster strain rates the rhyolite was non-Newtonian.

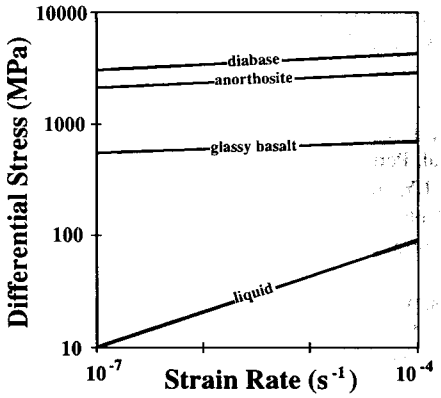

Fig. 8. Comparison at 825°C of strengths of diabase, anorthosite (Shelton and Tullis, 1981), glassy basalt (experiments in this study at ≥ 825°C), and rhyolite liquid (Webb and Dingwell, 1990) at experimental conditions. Note that the strength of the glassy basalt is a linear function of the strength of diabase or anorthosite and that rhyolite liquid is one to two orders of magnitude weaker.

We propose that the mechanical behavior of the high-temperature glassy basalt may be modeled as a porous aggregate because the strength of the melt at temperatures ≥ 825°C (predicted from the data of Webb and Dingwell, 1990) is more than an order of magnitude weaker than the strength of holocrystalline anorthosite and diabase (computed from Shelton and Tullis, 1981). The glassy basalt samples deformed at ≥ 825°C have strengths that are 26% of those calculated for anorthosite using Shelton and Tullis' (1981) constitutive relation. Alternatively, by comparison to the diabase deformed by Shelton and Tullis (1981), the high-temperature glassy basalt is 17% as strong. This direct linear strength decrease exists because the stress exponents for the high-temperature glassy basalt, anorthosite, and diabase are the same within measurement uncertainty.

An initial treatment of the strength of porous aggregates by Eudier (1962), considering equally spaced spherical pores, was subsequently expanded by Haynes (1971), Griffiths et al. (1979), and Tharp (1983). In this treatment, the pores are considered to reduce the strength of the aggregate by a factor related to an empirical constant λ, and the porosity, ϕ:

$$\sigma_{\text{porous}} = \sigma_{\text{nonporous}}(1 - \lambda\phi^{2/3})$$

Various metals with porosities of 15 vol.% have strengths that are $\sim 50\%$ of the strength of the non-porous metal (Haynes, 1971; Tharp, 1983), indicating $\lambda = 1.77$. However, Griffiths et al. (1979) noted that it is important to consider the shape of the pores, because non-spherical pores have greater stress concentrations and produce lower aggregate strengths. They predicted that the strength of a material containing 15 vol.% pores with 2.2:1 aspect ratios would be 36% of the strength of the non-porous material, i.e. $\lambda = 2.26$. Larger pore aspect ratios yield greater aggregate strength reductions (because of increased

stress concentrations) and higher λ values. The melt pockets in the glassy basalt vary in aspect ratio from 2:1 to 10:1, thus the appropriate λ values are likely > 2.26. Consequently, the strength of the glassy basalt at temperatures $\geq$ 825°C can reasonably be expressed as simple functions of anorthite or basalt strengths with λ of 2.62 or 2.94:

$$\sigma_{basalt} = \sigma_{anorthite}(1 - 2.62 * 0.15^{2/3})$$

$$\sigma_{basalt} = \sigma_{diabase}(1 - 2.94 * 0.15^{2/3})$$

It is more difficult to rationalize the mechanical behavior of the low-temperature ($\leq$ 775°C) glassy basalt in terms of a two-phase aggregate. Because the stress exponent for the low-temperature glassy basalt ($n = 5.4$) is significantly different than that of anorthosite and diabase (and the high-temperature glassy basalt as well), the strength of the low-temperature samples cannot be a simple linear fraction of the strength of those rocks. Moreover, because the strength of the melt (predicted from Webb and Dingwell, 1990) is grossly equivalent to the strength of anorthosite and diabase (predicted from Shelton and Tullis, 1981), the strength of the glassy basalt at temperatures $\leq$ 775°C must necessarily be a more complicated function of the rheology of the solid and melt phases. The strength of the glassy basalt is closer to the strength of diabase or anorthosite than the strength of melt at slower strain rates than at faster strain rates. This indicates that the rheological influence of the melt is greatest at faster strain rates, perhaps because the melt becomes non-Newtonian at faster strain rates (cf. Webb and Dingwell's rhyolite).

Conclusions

Experimental deformation of a glassy basalt occurred by melt-assisted cataclasis and dislocation creep. The cataclasis was concentrated in fault zones inclined $\sim 45°$ to the compression axis that formed by the coalescence of extensional fractures in plagioclase crystals. A glass $\rightarrow$ liquid transition(?) at $\sim$ 800°C caused a marked weakening. The crystallization of glass to mica and quartz appears to have promoted dislocation glide in plagioclase and suppressed cracking and twinning associated with unrecrystallized glass. The high strain-rate sensitivity of the sample strength suggests that dislocation glide or deformation of thin melt films (and not cracking) controlled the rate of deformation. The mechanical behavior of the glassy basalt at high temperatures can be modeled by assuming that the basalt is composed of a framework of plagioclase grains separated by $\sim$ 15 vol.% anisotropic liquid-filled pores.

Acknowledgements

These experiments were stimulated by some exploratory work on this basalt conducted at UCLA by Byong Ryol Choi, on leave from Chungbuk National University, Korea. This work was funded by NSF Grant EAR84-16781 to J.M.C. and a Sigma Xi research grant to B.R.H. Careful reviews by Jan Tullis and Lisa Dell'Angelo are gratefully acknowledged.

References

Avé Lallement, H.G., 1978. Experimental deformation of diopside and websterite. Tectonophysics, 48: 1–27.

Avé Lallement, H.G. and Carter, N.L., 1970. Syntectonic recrystallization of olivine and modes of flow in the upper mantle. Geol. Soc. Am. Bull., 81: 2203–2220.

Blacic, J.D., 1971. Hydrolitic weakening of quartz and olivine. Ph.D. thesis, Univ. California, Los Angeles, Calif., 205 pp.

Borch, R.S. and Green, H.W. II, 1989. Deformation of peridotite at high pressure in a new molten salt cell: comparison of traditional and homologous temperature treatments. Phys. Earth Planet. Inter., 55: 269–276.

Borg, I.Y. and Heard, H.C., 1969. Mechanical twinning and slip in experimentally deformed plagioclase. Contrib. Mineral. Petrol., 23: 128–135.

Borg, I.Y. and Heard, H.C., 1970. Experimental deformation of plagioclases. In Paulitsch (Editor) Experimental and Natural Rock Deformation. Springer, New York, pp. 375–403.

Brown, W.L. and Macaudiere, J., 1986. Mechanical twinning of plagioclase in a deformed meta-anorthosite—the production of M-twinning, Contrib. Mineral. Petrol., 92: 44–56.

Cooper, R.F. and Kohlstedt, D.L., 1984. Solution-precipitation enhanced diffusional creep of partially molten olivine-basalt aggregates during hot-pressing. Tectonophysics, 107: 207–233.

Dell'Angelo, L.N. and Tullis, J., 1988. Experimental deformation of partially melted granitic aggregates. J. Metamorph. Geol., 6: 495–515.

Dell'Angelo, L.N. and Tullis, J., 1989. Fabric development in experimentally sheared quartzites. Tectonophysics, 169: 1–21.

Dell'Angelo, L.N., Tullis, J. and Yund, R.A., 1987. Transition from dislocation creep to melt-enhanced diffusion creep in fine-grained granitic aggregates. Tectonophysics, 139: 325–332.

Eudier, M., 1962. The mechanical properties of sintered low-alloy steels. Powder Metall., 9: 278–290.

Getting, I.C. and Kennedy, G.C., 1970. The effect of pressure on the e.m.f of chrome-alumel and platinum–platinum 10% rhodium thermocouples. J. Appl. Phys, 41: 4552–4561.

Griffiths, T.J., Davies, R. and Bassett, M.B., 1979. Analytical study of effects of pore geometry on tensile strength of porous materials. Powder Metall., 22: 119–123.

Griggs, D.T., 1967. Hydrolitic weakening of quartz and other silicates. Geophys. J. R. Astron. Soc., 14: 19–31.

Hacker, B.R. and Christie, J.M., 1990. Brittle/ductile and plastic/cataclastic transitions in experimentally deformed and metamorphosed amphibolite. Am. Geophys. Union, Monogr., 56: 127–147.

Hacker, B.R. and Kirby, S.H., 1990. Effect of stress and deformation on albite breakdown. Eos, Trans. Am. Geophys. Union, 71: 639.

Hacker, B.R., Christie, J.M. and Choi, B.R., 1987. The rheology of basaltic rocks and the implications for deformation and metamorphism in subduction zones. Geol. Soc. Am., Abstr. Progr., 19: 689.

Haynes, R., 1971. Effect of porosity content on the tensile strength of porous materials. Powder Metall., 14: 64–70.

Jordan, P., 1988. The rheology of polymineralic rocks. Geol. Rundsch., 77: 285–294.

Kirby, S.H., 1987. Localized polymorphic phase transitions in high-pressure faults and applications to the physical mechanism of deep earthquakes. J. Geophys. Res., 92; 13789–13800.

Kirby, S.H. and Kronenberg, A.K., 1984. Deformation of clinopyroxenite: evidence for a transition in flow mechanisms and semi-brittle behavior. J. Geophys. Res, 89: 3177–3192.

Koch, P.S., Christie, J.M., Ord A. and George, R.P., Jr., 1989. Effect of water on the rheology of experimentally deformed quartzite. J. Geophys. Res., 94: 13975–13996.

Kollé, J.J. and Blacic, J.D., 1982. Deformation of single-crystal clinopyroxenes: 1. Mechanical twinning in diopside and hedenbergite. J. Geophys. Res., 87: 4019–4034.

Kollé, J.J. and Blacic, J.D., 1983. Deformation of single-crystal clinopyroxenes: 2. Dislocation-controlled flow in hedenbergite. J. Geophys. Res., 88: 2381–2393.

Kronenberg, A.K. and Shelton, G.L., 1980. Deformation microstructures in experimentally deformed Maryland diabase. J. Struct. Geol., 2: 341–353.

Mao, H.K. and Bell, P.M., 1971. Behavior of thermocouples in the single-stage piston-cylinder apparatus, Carnegie Inst. Washington, Yearb. 69: 207–216.

Marshall, D.B. and MacLaren, A.C., 1977a. Deformation mechanisms in experimentally deformed plagioclase feldspars. Phys. Chem. Miner., 1: 351–370.

Marshall, D.B. and MacLaren, A.C., 1977b. The direct observation and analysis of dislocations in experimentally deformed plagioclase feldspars. J. Mater. Sci., 12: 893–903.

Merzbacher, C. and Eggler, D.H., 1984. A magmatic geohygrometer: application to Mount St. Helens and other dacitic magmas. Geol., 12: 587–590.

Murrell, S.A.F. and Ismail, I.A.H., 1976. The effect of decomposition of hydrous minerals on the mechanical properties of rocks at high pressures and temperatures, Tectonophysics, 31: 207–258.

Nissen, H.-U., 1974. Exsolution phenomena in bytownite plagioclases. In: W.S. MacKenzie and J. Zussman (Editors), The Feldspars. Manchester University Press, New York, pp. 491–521.

Peterson, J.W. and Newton, R.C., 1990. Experimental biotite-quartz melting in the KMASH–CO_2 system and the role of CO_2 in the petrogenesis of granites and related rocks. Am. Mineralog., 75:1029–1041.

Raleigh, C.B. and Paterson, M.S., 1965. Experimental deformation of serpentinite and its tectonic implications. J. Geophys. Res., 70: 3965–3985.

Riecker, R.E. and Rooney, T.P., 1966. Weakening of dunite by serpentine dehydration. Science, 152: 196–198.

Rutter, E.H. and Brodie, K.H., 1988. Experimental "syntectonic" dehydration of serpentinite under conditions of controlled pore water pressure, J. Geophys. Res., 93, 4907–4931.

Seifert, K. E. and VerPloeg, A.J., 1977. Deformation characteristics of experimentally deformed Adirondack anorthosite. Can. J. Earth Sci., 14: 2706–2717.

Shea, W.T. and Kronenberg, A.K., 1989. Experimental deformation of biotite schist. Eos, Trans. Am. Geophys. Union 70: 477.

Shelton, G.L. and Tullis, J., 1981. Experimental flow laws for crystal rocks. Eos, Trans. Am. Geophys. Union 62: 396.

Shelton, G.L., Tullis, J. and Tullis, T., 1981. Experimental high temperature and high pressure faults. Geophys. Res. Lett., 8: 55–58.

Smith, J.V., 1989. Phase relations of plagioclase feldspars. In: W.L. Brown (Editor), Feldspars and Feldspathoids. Reidel, Dordrecht, pp. 54–94.

Stern, C.R., Huang W.-L. and Wyllie, P.J., 1975. Basalt–andestie–rhyolite–H_2O: crystallization intervals with excess H_2O and H_2O-undersaturated liquidus surfaces to 35 kilobars, with implications for magma genesis. Earth Planet. Sci. Lett., 28: 189–196.

Tharp, T.M., 1983. Analogies between the high-temperature deformation of polyphase rocks and the mechanical behavior of porous powder metal. Tectonophysics, 96: T1–T11.

Tullis, J. and Yund, R.A., 1977. Experimental deformation of dry Westerly granite. J. of Geophys. Res., 82: 5705–5718.

Tullis, J. and Yund, R.A., 1980. Hydrolitic weakening of experimentally deformed Westerly granite and Hale albite rock. J. Struct. Geol., 2: 439–451.

Tullis, J. and Yund, R.A., 1987. Transition from cataclastic flow to dislocation creep of feldspar: Mechanisms and microstructures. Geology, 15: 606–609.

Van der Molen, I. and Paterson, M.S., 1979. Experimental deformation of partially-melted granite. Contrib. Mineral. Petrol., 70: 299–318.

Webb, S.L. and Dingwell, D.B., 1990. Non-Newtonian rheology of igneous melts at high stresses and strain rates: experimental results for rhyolite, andesite, basalt, and nephelinite. J. Geophys. Res., 95: 15695–15701.